Radar mapping of lunar cryptomaria east of Orientale basin

Bruce A. Campbell
Center for Earth and Planetary Studies, Smithsonian Institution, Washington, D. C., USA

B. Ray Hawke
Hawai'i Institute of Geophysics and Planetology, University of Hawai'i at Manoa, Honolulu, Hawaii, USA

Received 28 February 2005; revised 22 June 2005; accepted 27 June 2005; published 7 September 2005.

[1] Lunar cryptomare deposits represent early basaltic volcanic material that has been mantled by or incorporated into highland-rich ejecta from basin- or crater-forming impacts. Mapping these buried basalts is important for understanding regional stratigraphy and the history and extent of lunar volcanism. We use new 70 cm wavelength radar images, collected using Arecibo Observatory and the Green Bank Telescope, and Clementine data to study cryptomaria east of Orientale basin. Earlier multispectral analyses showed that mare material is mixed with the highland terrain along the western margin of Oceanus Procellarum, leading to a detectable increase in the FeO and TiO_2 abundance of the regolith surface. The highland margin of western Procellarum is also characterized by low 70 cm radar returns, consistent with an increased regolith loss tangent due to ilmenite in the mare-derived material. The low 70 cm radar echo, however, persists well to the west of the mixed zone evident in multispectral data and includes the region surrounding Cruger crater. It is likely that mare basalt, or a mixed zone of mare and highland material, exists at depth across the region and only reaches the visible surface near the western Procellarum margin. The plausible depth to this mixed zone is dependent upon the loss tangent of the overlying "pure" highland ejecta. If Orientale ejecta is primarily low-loss anorthosite, then the mixed zone could lie at depths of up to several tens of meters. We propose that pre-Orientale mare deposits flooded the region between Cruger, Grimaldi, and Oceanus Procellarum and also patches west and northwest of Humorum basin. The total area of these deposits represents 178×10^3 km^2, or an additional ~0.5% of the lunar surface, covered by mare basalts.

Citation: Campbell, B. A., and B. R. Hawke (2005), Radar mapping of lunar cryptomaria east of Orientale basin, *J. Geophys. Res.*, *110*, E09002, doi:10.1029/2005JE002425.

1. Introduction

[2] Basaltic volcanism on the Moon followed the development of a feldspathic crust from the early magma ocean and typically filled large impact basins to form the maria. Most of the known mare deposits lie on the nearside of the Moon, with smaller patches in farside basins and craters. In some regions, early mare volcanism has been mantled by or incorporated into ejecta deposits from later basin- or crater-forming impacts. Such deposits, termed "cryptomaria," have been identified on the basis of two criteria: (1) small craters that excavate the buried basalt, creating a characteristic dark halo in visible images [e.g., *Schultz and Spudis*, 1979; *Antonenko et al.*, 1995], and (2) variations in the multispectral signature of highland terrain, which indicate preexisting mare material has been incorporated into the basin ejecta [e.g., *Mustard and Head*, 1996]. Such techniques have been used to identify likely cryptomare deposits west of Oceanus Procellarum [*Mustard and Head*, 1996], northwest of Mare Humorum [*Lucey et al.*, 1991; *Hawke et al.*, 1993], in the "Schiller-Schickard" region [*Blewett et al.*, 1995], in the Balmer basin [*Hawke et al.*, 2004], and within the Australe basin [*Antonenko et al.*, 1995].

[3] These studies rely on the UV, visible, and near-infrared reflectance properties of the regolith surface and on excavation of buried material by small "dark halo craters" (DHC). The multispectral approach is limited to mare-highland mixtures that reach the visible surface and by the uncertainty in estimating, for example, FeO or TiO_2 at very low abundance [*Lucey et al.*, 2000]. The DHC approach provides only "point measurements" of areally distributed cryptomaria. Long-wavelength radar can provide complementary information by probing to depths of meters to tens of meters to study the bulk dielectric properties and decimeter-scale rock abundance of the regolith. Past work shows that 70 cm wavelength radar echoes, particularly in the "depolarized" or same-sense circular (SC) polarization, are sensitive to the abundance of lossy minerals (such as ilmenite), which modulate the bulk loss tangent of the regolith [e.g., *Schaber et al.*, 1975; *Campbell et al.*, 1997]. Radar echoes are also relatively insensitive to the small-scale

0148-0227/05/2005JE002425$09.00

changes in regolith texture and near-surface chemistry that comprise "maturation" and to the thin layers of ejecta from distant impact craters.

[4] In this paper, we use new high-resolution (450 m pixel^{-1}), 70 cm wavelength radar images to study the region between Orientale basin and Oceanus Procellarum and to identify the boundaries of cryptomaria through their effect on the bulk loss tangent of mixed highland-mare debris layers. Section 2 details the radar observations. Section 3 presents a comparison of radar and multispectral data for the study region and notes the differences in behavior between areas previously identified as mixed mare and highlands and our more extensive proposed cryptomare deposit. Section 4 discusses the effects of surface roughness, subsurface rock population, and regolith geochemical properties on the backscattered return and suggests a plausible range of depths for a lossy (mixed mare-highland) layer. Section 5 integrates the radar and multispectral data to offer a new geologic synthesis for the region.

2. Lunar Radar Mapping at 70 cm Wavelength

[5] We collect 70 cm wavelength (430 MHz frequency), dual-circular polarization backscatter maps of the Moon by transmitting a 3 μs pulse from the 305 m Arecibo telescope and receiving the echoes at the 105 m Green Bank Telescope (GBT) in West Virginia. The surface horizontal resolution along the range axis is a function of the pulse length and radar incidence angle ϕ; resolution is ~900 m at 30° incidence and ~450 m at the limbs. Spatial resolution along the frequency axis is a function of the integration time for each look, which sets the frequency resolution, and the angular offset of any point from the apparent spin axis of the Moon, which determines the projected resolution cell size. The total integration time for each look is 983 s for a frequency resolution of ~1 mHz. The Moon has a limb-to-limb bandwidth at 430 MHz of ~11 Hz, so our best spatial resolution along the frequency axis is ~320 m. All maps are produced at 400 m pixel spacing to minimize under sampling and represent averages over three or more independent looks to reduce speckle and thermal noise effects.

[6] Each radar look is normalized to the receiver noise level measured at delay times before or after the lunar echoes. We can thus calibrate the power ratio between the same-sense (SC) and opposite-sense (OC) circular polarization states. We also correct for the variation in antenna beam sensitivity across the images, using a best fit beam pattern determined from overlap regions of images collected for different targets. Absolute calibration efforts, using sky sources of known radio brightness and measurements of the transmitted power level, are in progress; all backscatter coefficient σ^0 values cited here are relative to an arbitrary absolute reference level. Since all of the radar data come from the same observing run, the relative calibration between backscatter values across the image area is very good.

[7] The opposite-sense echo comprises mirror-like (quasi-specular) reflections from favorably oriented portions of the surface and diffuse reflections from rocks or other features on the scale of the radar wavelength. The same-sense echo is dominated by the diffuse component. In both cases the scattering elements (e.g., rocks) may be on the surface or buried within the regolith. Longer radar wavelengths probe to greater depths and are sensitive to scattering by the larger objects in a size-frequency distribution (typically greater than ~1/10 the wavelength). The effective probing depth is determined by the microwave loss tangent of the regolith, which depends upon the mineralogy (especially the ilmenite abundance) of the constituent materials.

[8] The delay-Doppler radar data are projected to a latitude-longitude format by a 3 × 3 matrix transform that links the apparent Cartesian coordinate system created by the Moon's spin and libration with the cartographic framework. At any given instant the Moon's apparent motion may be described by (1) a subradar point location (latitude, longitude), (2) a rotation rate or limb-to-limb bandwidth, and (3) a spin axis orientation angle. We solve for these parameters by an iterative fit to ephemeris data for three or more locations on the lunar surface. The ephemerides are updated for each minute, so we create a polynomial fit for the variation of the Moon's spin state as a function of time.

[9] The radar is "pointed" by tracking a particular location on the Moon's surface, such that the transmitted signal is adjusted to maintain the target at zero apparent Doppler shift and delay. Other points on the Moon's surface are translating, at varying rates, with respect to the target. With the fits to the Moon's spin state we may calculate this time-dependent differential delay and frequency shift for any chosen point and remove it from the raw complex data array. When mapped, the resulting image is focused for an area around the chosen location. In practice, we map the region illuminated by the antenna beam in small (120 × 120 km) patches to obtain a focused image with the best possible spatial resolution.

3. Radar and Multispectral Data for the Orientale-Procellarum Region

3.1. General Properties

[10] The region between Orientale basin and Oceanus Procellarum (Figure 1) is characterized by relatively high albedo terrae, emplaced as ejecta during the basin-forming impact. The ejecta deposits vary in thickness and morphology with distance from the basin center; the "inner Hevelius formation" is characterized by thick lobes and large-scale sculpture, and the "outer Hevelius formation" represents thinner lobes and smooth, light plains [*Scott et al.*, 1977; *Wilhelms*, 1987; *Bussey and Spudis*, 2000]. Post-Orientale mare deposits, typically of low relief and low relative albedo, fill Oceanus Procellarum, Cruger crater, Grimaldi basin, and a number of smaller topographic lows. There are also mare patches within the Orientale basin floor and ring structures.

[11] A study by *Mustard and Head* [1996], using Galileo multispectral data, shows that the highland terrain along the western margin of Oceanus Procellarum is contaminated by mafic material. They attribute this to a series of geologic events: (1) the emplacement of pre-Orientale mare basalts, (2) the Orientale impact that buried these mare deposits and incorporated mafic material into some parts of the basin ejecta, (3) basaltic flooding of Oceanus Procellarum, and (4) lateral mixing of Procellarum basalts with the highlands by small impacts.

[12] The spectral signature of the highland mafic contamination, identified by *Mustard and Head* [1996], decays

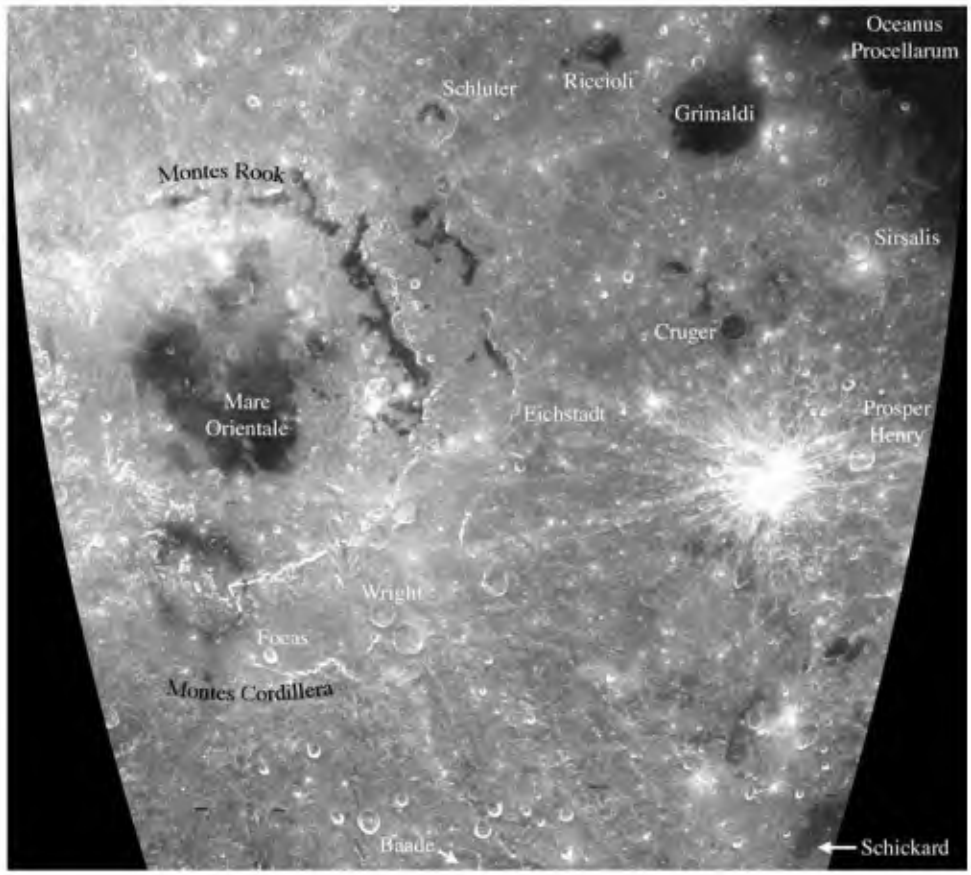

Figure 1. Clementine 750 nm image of the region from Orientale basin to western Oceanus Procellarum (0°–45°S, 55°–105°W).

rapidly with distance westward from Procellarum, and only a relatively small number of dark halo craters have been identified in the region [*Schultz and Spudis*, 1979]. Work by *Hawke et al.* [1993] identifies likely mafic contamination, indicating prebasin mare deposits, in the terrain NW of Humorum, SE of our study region. There is thus good reason to suspect that pre-Orientale mare basalts exist near the Procellarum margin and northwest of Humorum, but there is little evidence (e.g., DHCs) to date that such deposits extend farther west.

[13] The new 70 cm radar data provide a complementary view of the Orientale-Procellarum region (Figure 2). The radar echo is generally low in areas covered by basalt and is high in the terrae (the inner Hevelius formation) adjacent to the outer cordillera ring of Orientale. Surrounding Cruger crater and extending east toward Oceanus Procellarum, northwest toward Grimaldi basin, and southeast toward Mare Humorum, however, there is an extensive region of low radar return that is anticorrelated with the high visible albedo of the surface. This area generally corresponds to the outer facies of the Orientale-derived Hevelius formation [*Scott et al.*, 1977]. The long-wavelength radar signal is not sensitive to maturity differences or ray-like ejecta, so we can trace these low-return areas close to even young impact craters. Outlying radar-dark regions are also observed, for example, surrounding Rocca P crater (Figure 3). There are also several areas of low radar echo south of Cruger and extending to the region northwest of Schickard crater.

[14] Radar images are also available at wavelengths of 3.8 cm and 7.5 m [*Zisk et al.*, 1974; *Thompson*, 1978]. The 3.8 cm signal penetrates at most ~1 m into even low-loss highland material and is more affected by the surface and near-surface rock abundance than by the bulk regolith loss tangent. Since we are concerned here with deep penetration and probing of possible mixed highland and mafic materials, we focus on the longer-wavelength radar data. In the 7.5-m wavelength image (10–30 km resolution), there is a distinct region of decreased radar echo east of Cruger, separated from Oceanus Procellarum by a SE-NW trending band of higher, terra-like returns (Figure 4). The low-return area around Cruger is consistent with the extent of the 70 cm radar low.

3.2. Radar-Multispectral Correlations

[15] We coregistered the Clementine five-band UV–visible multispectral data set to the 70 cm data to examine the variation of radar backscatter in the SC (or depolarized) mode with FeO (Figure 5) and TiO_2 (Figure 6) abundances derived by the methods of *Lucey et al.* [2000] and *Gillis et al.* [2003]. The SC radar echoes are normalized prior to averaging by $\cos^{1.5}\phi$, where ϕ is the radar incidence angle, to reduce variations in backscatter with viewing geometry. We examined the dependence of radar backscatter on model-derived FeO and TiO_2 abundance for four sample regions (Figure 7). The average backscatter values (dB) across each sample region are plotted as a

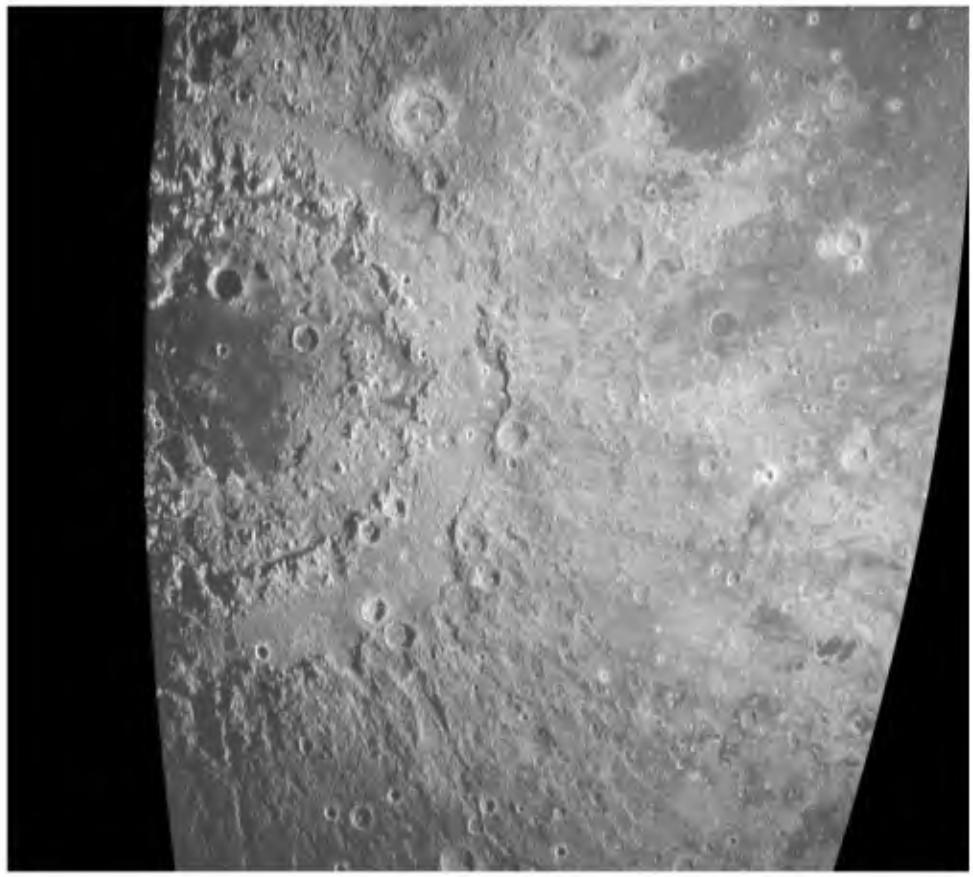

Figure 2. The 70 cm same-sense polarization (depolarized) radar map of the Orientale-Procellarum study region (0°–45°S, 55°–105°W). Antenna beam pattern gain sensitivity removed; no-scattering law removed, so the image darkens toward the limb.

function of FeO (Figure 8a), TiO_2 (Figure 8b), and FeO+TiO_2 (Figure 8c) weight percentage.

[16] In the maria of western Oceanus Procellarum we observe a decline in average backscatter strength with increasing TiO_2 content, consistent with previous studies of the effect of ilmenite on the loss tangent of lunar materials [*Schaber et al.*, 1975; *Carrier et al.*, 1991; *Campbell et al.*, 1997]. There is also a decline in backscatter with increasing FeO abundance, though the range of iron content is much smaller than for the titanium. In the "pure" terrae of the inner Hevelius formation we observe a similar drop in echo power with increasing TiO_2, but the overall backscatter is much higher (by ~6 dB, or a 3:1 ratio) than for the maria. This large difference in radar echo power between the terrae and maria has been attributed to lower microwave losses in the highlands, which permit a probing wave to interact with buried rocks over a much longer path length.

[17] The region between Grimaldi and Oceanus Procellarum, identified by *Mustard and Head* [1996] as mixed mare and highlands, has properties intermediate between the pure terrae and maria. At low TiO_2 and FeO abundance the radar echoes are similar to those of the inner Hevelius formation. As the iron and titanium content increases, the radar echo declines toward those of the western Procellarum mare deposits. The radar results thus support the interpretation of this region as underlain by mare basalts that are mixed, to varying degrees, with the overlying highland-dominated

Figure 3. Lunar Orbiter 4 and 70 cm same-sense polarization radar map (inset) of Rocca P crater and the area southwest of Grimaldi basin. Regions of low radar backscatter shown by arrows in inset map.

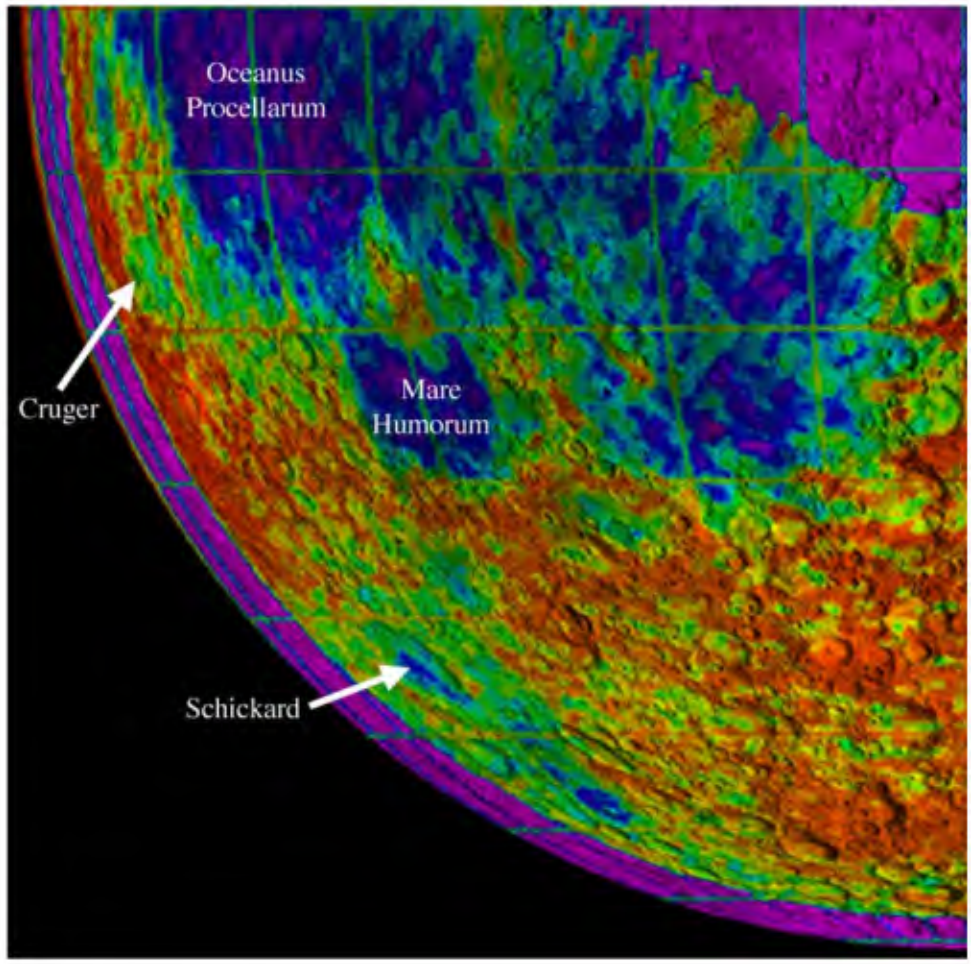

Figure 4. The 7.5 m opposite-sense circular polarized radar map of the SW quadrant of the lunar nearside, showing the area of low return associated with the region between Cruger crater and Oceanus Procellarum. Spatial resolution 10–30 km [*Thompson*, 1978]. Orthographic projection. Color overlay of radar return on U.S. Geological Survey shaded relief image (lower returns purple or blue; moderate echoes green; high returns red).

regolith. Overall, these three areas appear to define a simple trend of decreasing radar echo with increasing iron and titanium content (Figure 8c), which we attribute primarily to the role of ilmenite in modulating the microwave loss tangent of the regolith.

[18] The region near Cruger and Sirsalis craters is very different from our other three sample areas. The dependence of backscatter on TiO_2 and FeO abundance follows a similar trend to that defined by the inner Hevelius and Grimaldi-Procellarum areas, but the overall radar brightness is 5–6 dB less than the terra echo. Similar properties characterize the radar-dark deposits surrounding Rocca P crater and south of Grimaldi basin. In essence, these areas have multispectral properties consistent with basin-derived highland ejecta, but a mare-like 70 cm radar echo.

4. Radar Scattering From the Lunar Regolith

4.1. General Model

[19] We observe radar echoes associated with possible cryptomare deposits that are typically lower than those of pure highland material. In this section we develop a simple model for regolith radar scattering that provides a context for a comparison of backscatter and geochemical properties. Radar echoes from the lunar regolith are affected by a number of factors: the complex dielectric constant of the dust and rock, the surface and subsurface rock population, and the possible presence of a lossy layer or basal interface within the probing range of the radar signal. We examine three possible scenarios that could lead to lower radar echoes: (1) a reduction in the volume rock population, (2) an intimate mixture of highland and mare material, and (3) burial of lossy mare material by highland debris.

[20] The backscattered radar echo is composed of surface and subsurface contributions. The surface echo arises from quasi-specular reflections from topography on horizontal scales several or more times the illuminating wavelength λ and from diffuse reflections from rock faces and edges smaller than a few wavelengths across. The subsurface return is dominated by reflections from faces or edges of rocks suspended in the fine-grained matrix. Except for very young, very low TiO_2 maria it is unlikely that radar echoes for $\lambda < 1$ m contain a strong component arising from reflections by a basal regolith interface (e.g., the actual lava

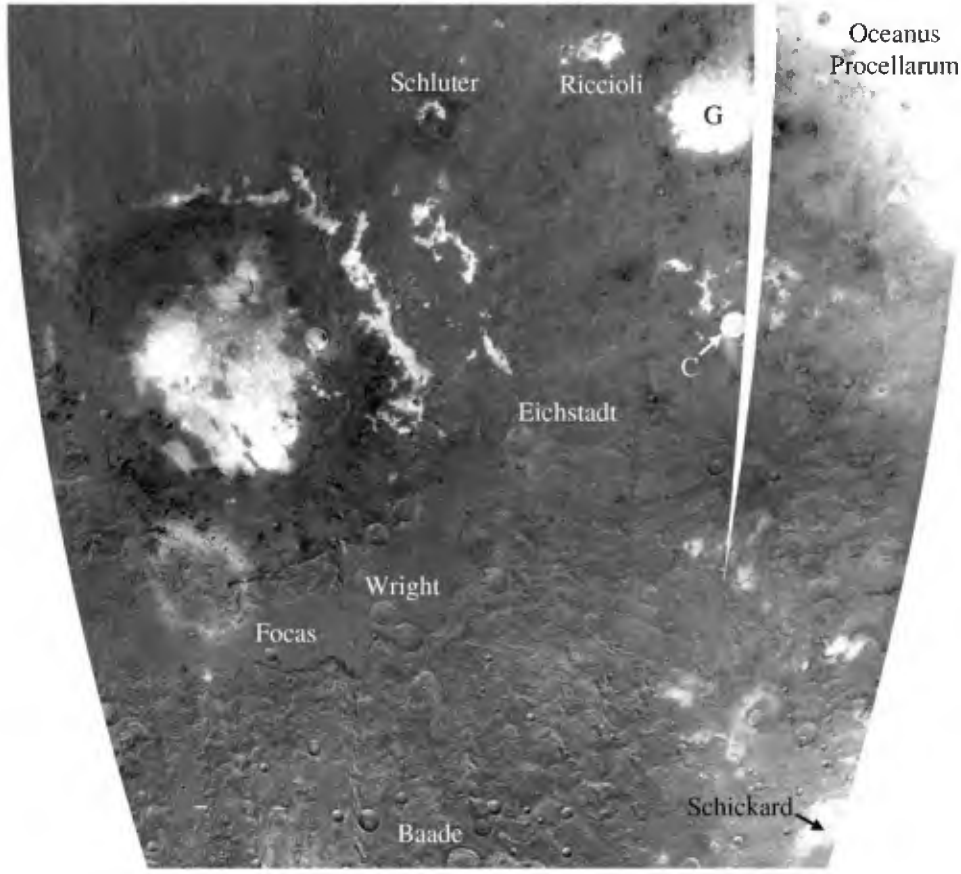

Figure 5. FeO weight percent map of the study region, derived from the algorithm of *Lucey et al.* [2000]. Image stretch (black = 0%, white > 15%). Note the FeO-rich ring of pyroclastic deposits south of Orientale (NW of Focas crater). C, Cruger crater; G, Grimaldi basin.

flow surface) [*Campbell*, 2002]. The quasi-specular component contributes only to the OC polarization echo. The surface and subsurface diffuse return is split between SC and OC polarizations, with small rock faces contributing more strongly to the OC echo and rock edges contributing approximately equal SC and OC returns [e.g., *Hagfors*, 1967; *Stacy*, 1993; *Campbell et al.*, 1993]. Subsurface reflections are strongly affected by the loss tangent tan δ and volume rock population of the regolith, which together determine the effective penetration depth and the number of rocks encountered by a probing signal. The subsurface return is also reduced by Fresnel transmission at the space-regolith interface.

[21] We may represent the total SC (depolarized) backscatter echo from the regolith as

$$\sigma^0_{SC} = \sigma^0_{surface} + \sigma^0_{subsurface}, \tag{1}$$

where the surface echo is related to the subsurface echo by assuming that the surface rock population represents a "slice" through a well-mixed three-dimensional distribution [*Shoemaker and Morris*, 1968]. For a layer of thickness h (where h is at least several times the largest reasonable scattering object) the net subsurface return is approximated by

$$\sigma^0_{subsurface} = \frac{T\cos\theta}{4\alpha}\left[1 - \exp\left(\frac{-4\alpha h}{\cos\theta}\right)\right]\sigma^0_{rocks}. \tag{2}$$

T is the net (round-trip) Fresnel transmission coefficient for the space-regolith interface, θ is the radar incidence angle within the medium, and α is a loss factor approximated by

$$\alpha \approx \frac{\pi\sqrt{\varepsilon'}\tan\delta}{\lambda}, \tag{3}$$

where ε' is the real dielectric constant of the regolith, λ is the free space radar wavelength [*Ulaby et al.*, 1982], and σ^0_{rocks} is the integrated backscatter coefficient, in the polarization state of interest, of the volume rock population within the layer [*Campbell*, 2002]. The surface echo is related to σ^0_{rocks} by a multiplicative factor, largely dependent upon the dielectric contrast between rocks and dust, which we will term K:

$$\sigma^0_{SC} = \sigma^0_{rocks}\left\{K + \frac{T\cos\theta}{4\alpha}\left[1 - \exp\left(\frac{-4\alpha h}{\cos\theta}\right)\right]\right\} \tag{4}$$

If the scattering layer is thick with respect to the penetration depth of the radar, then the exponential term and the associated dependence of backscatter on layer thickness h vanish. In general, the proportion of surface echo will increase as the illuminating wavelength decreases (e.g., from 70 to 3.8 cm) since there are more

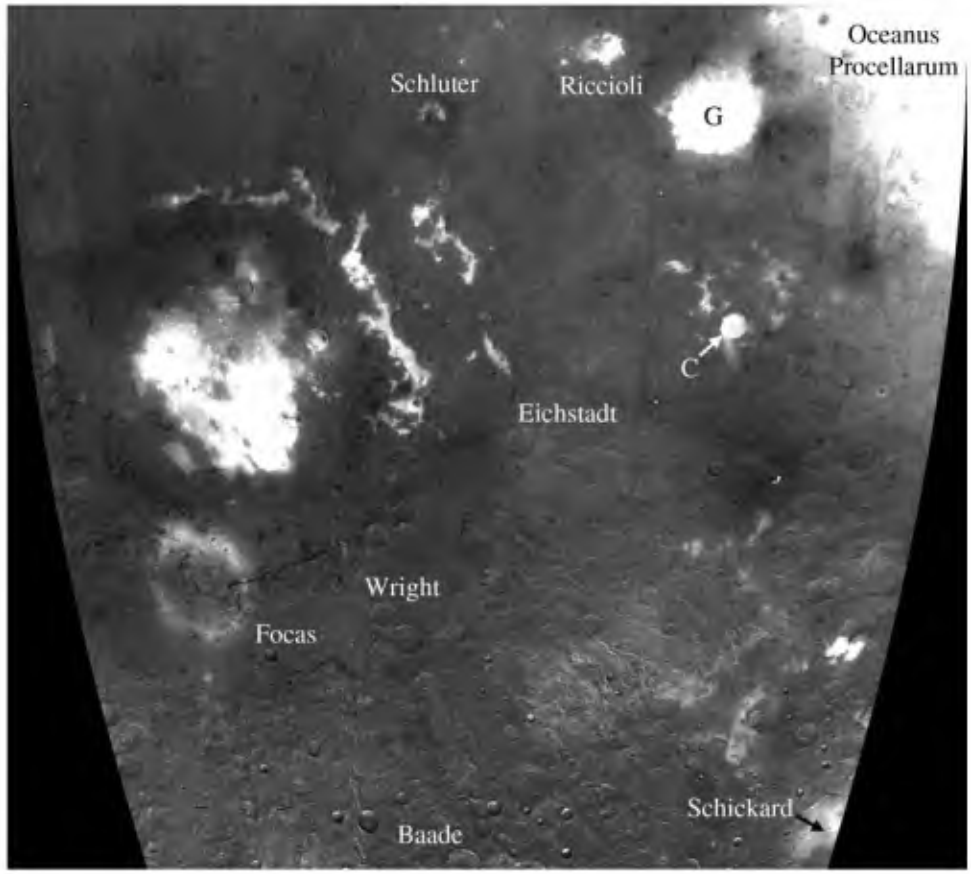

Figure 6. TiO_2 weight percent map of the study region, derived from the algorithm of *Gillis et al.* [2003]. Image stretch (black = 0%, white > 6%). C, Cruger crater; G, Grimaldi basin.

abundant small rocks near the surface to scatter the incident signal.

4.2. Volume Rock Population of the Lunar Regolith

[22] In a highland regolith the initial rock population associated with ejecta from a given basin is a function of the comminution of debris during the primary and secondary impacts and may vary with radial distance from the basin center. In the maria the regolith is developed by overlapping small impacts, which create a mixed dust and fragmental debris layer. Mare rock abundance varies considerably with the age of the basalts [e.g., *Shorthill*, 1973; *Campbell et al.*, 1997]. Younger mare flows have thin regolith cover, allowing smaller impacts to excavate a greater proportion of "fresh" fragmental bedrock. With increasing time the mare regolith thickens, and the volume rock population stabilizes at a lower level. In general, the near-surface rock population is lower in the terrae than in the maria because of the greater age of the deposits and the lack of a shallow "reservoir" of solid material to generate new fragmental debris.

4.3. Dielectric Properties of the Lunar Regolith

[23] The range of dielectric properties for lunar materials is known from remote sensing measurements and laboratory analyses of returned samples. From backscatter measurements and laboratory studies the average real dielectric constant of the lunar regolith is ~2.8, with only minor

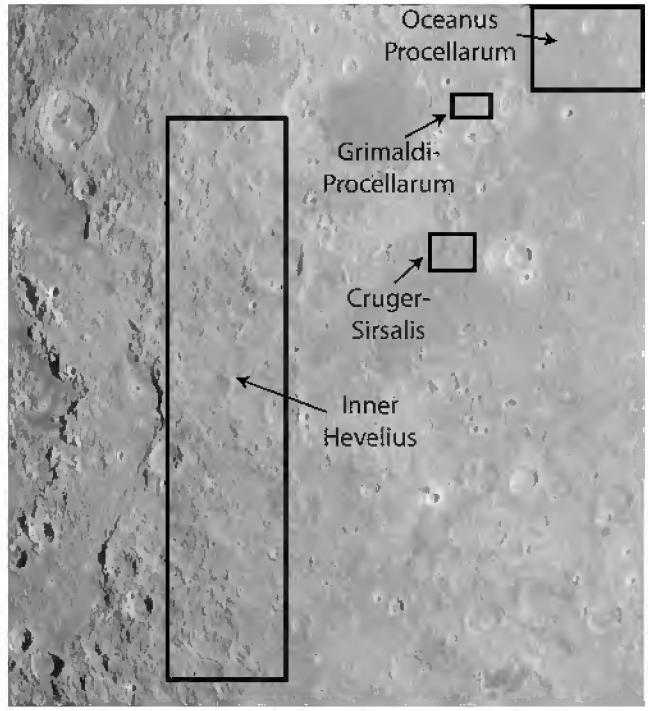

Figure 7. Sample regions for plots shown in Figure 8, noted on same-sense circular polarization radar image.

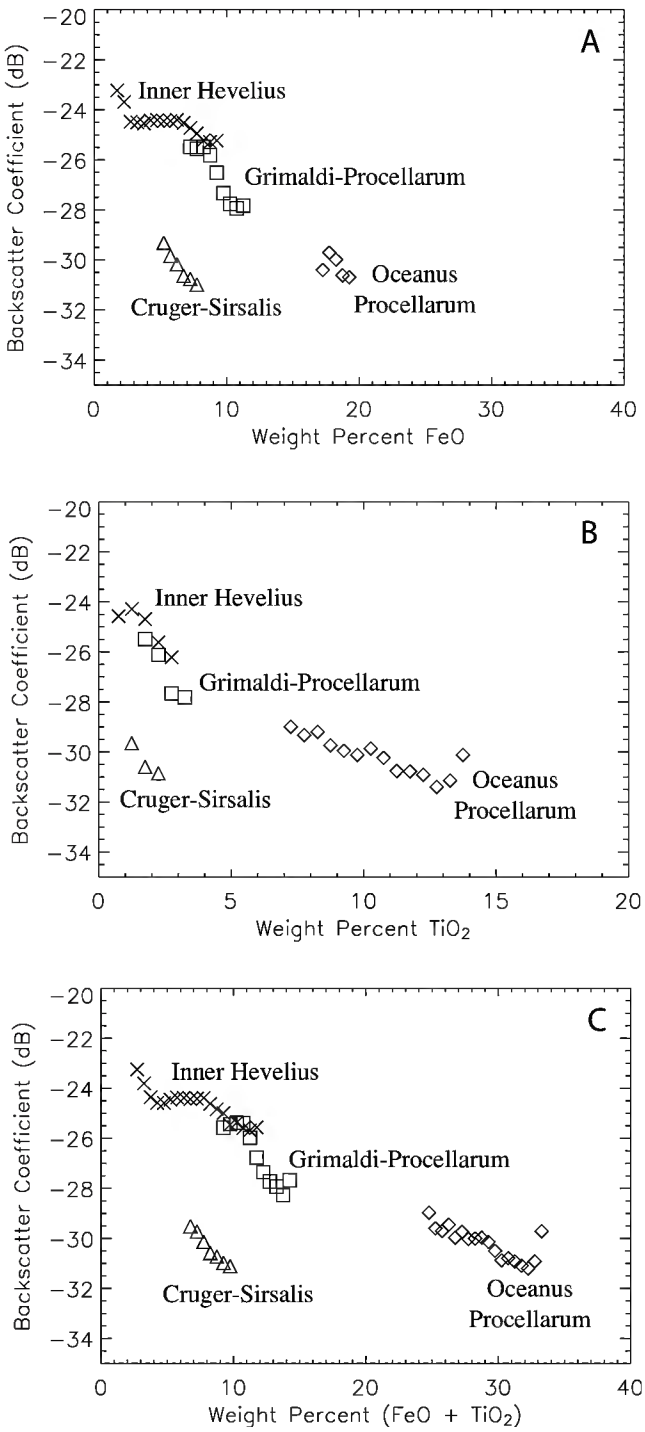

Figure 8. Average same-sense circular polarization radar backscatter coefficient (in decibels relative to an arbitrary reference level) versus (a) FeO, (b) TiO_2, and (c) FeO + TiO2 weight percentage for sample areas noted in Figure 7.

variations due to changes in bulk density between mare and highland material [e.g., *Hagfors*, 1970; *Carrier et al.*, 1991]. Such changes do not have a significant effect on our analysis. While there are likely contributions to the bulk loss tangent of the regolith from iron grains in agglutinates and other titanium- or iron-bearing minerals, the principal cause of variations in tan δ across the Moon appears to be ilmenite ($FeTiO_3$) abundance [*Schaber et al.*, 1975; *Campbell et al.*, 1997]. *Carrier et al.* [1991] cite a fit to the loss tangent of lunar samples as a function of the bulk (FeO + TiO_2) fraction:

$$\log_{10}(\tan\delta) = 0.03(\%TiO_2 + \%FeO) - 2.699. \quad (5)$$

This expression does not, however, reflect the loss tangents associated with rocks of very low iron and titanium content, which can have tan δ as low as 0.0002 [*Olhoeft and Strangway*, 1975].

4.4. Scenario 1: A Reduction in Volume Rock Population

[24] A reduction in the block population of the regolith is a very effective means for reducing the radar return since it affects both the surface and subsurface echo components through the σ^0_{rocks} term in (4). For example, many Imbrian, Eratosthenian, and Copernican craters have concentric "haloes" of low radar return and low circular polarization ratio μ_c that are distal to the rugged, radar-bright, near-rim ejecta. On the basis of the lack of any associated geochemical variations and the observation of low thermal infrared signatures for some of the haloes, *Ghent et al.* [2005] conclude that these concentric deposits reflect ejecta that is more comminuted (rock-poor) than the average background regolith. Over time, small impacts penetrate and garden the rock-poor halo areas; craters older than the Imbrian period therefore have no strong associated haloes.

[25] Is a rock-poor layer a reasonable mechanism for the low radar returns across the entire Cruger-Sirsalis-Procellarum region? There are numerous radar-dark haloes around younger impact craters in our study area, which we map in section 5. While some of these haloes occur between Cruger crater and Oceanus Procellarum, their total areal extent appears insufficient to explain the low 70 cm return across this region.

4.5. Scenario 2: Intimate Mixing of Highland and Mare Material

[26] If preexisting mare basalt and basalt-derived regoliths are incorporated into the ejecta curtain during basin formation, the mixed layer will have a higher bulk loss tangent than pure material excavated from the target highlands. This leads to an increase in the loss factor α (3) and an overall reduction in radar echo power for a given rock population (4). We may write the ratio of cryptomare backscatter to that of highland-dominated ejecta as

$$\frac{\sigma^0_{cryptomare}}{\sigma^0_{ejecta}} = \frac{K_{cryptomare} + \dfrac{T\cos\theta}{4\alpha_{cryptomare}}}{K_{ejecta} + \dfrac{T\cos\theta}{4\alpha_{ejecta}}}, \quad (6)$$

where we assume no change in the real dielectric constant and thus no difference in T or θ. The maximum possible difference in backscatter occurs when all of the scattering arises in the subsurface, for which $K_{cryptomare} \sim K_{ejecta} \sim 0$, so we may limit the ratio as

$$\frac{\sigma^0_{cryptomare}}{\sigma^0_{ejecta}} \le \frac{\alpha_{ejecta}}{\alpha_{cryptomare}} = \frac{\tan\delta_{ejecta}}{\tan\delta_{cryptomare}}. \quad (7)$$

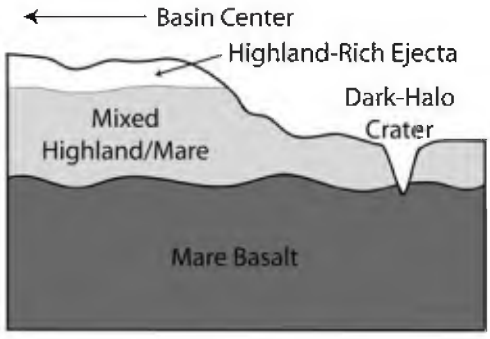

Figure 9. Schematic of radar-scattering model for cryptomaria between Orientale and Oceanus Procellarum. The mixed zone of mare and highland debris reaches the surface only near the highland margin of Procellarum.

[27] By substituting (5) into (7) we may show that each 1% change in ilmenite content leads to a maximum 0.6 dB drop in backscattered power for the volume-scattered component. The net drop in power between any two sites with different loss tangents is, however, diminished by the role of surface scattering. For example, if half of the observed echo arises from surface reflections, we will measure only ~0.3 dB difference in power for each 1% change in ilmenite content.

[28] Since we assume a well-mixed regolith, this scenario implies a strong correlation between radar echoes and TiO_2 abundance, inferred from multispectral data, and appears to be an excellent model for the inner Hevelius, Grimaldi-Procellarum, and Oceanus Procellarum sample regions (Figure 8b). The average backscatter coefficient drops by ~0.5 dB per weight percent of TiO_2, suggesting primarily subsurface scattering. This model does not, however, explain the properties of the Cruger-Sirsalis region or the other radar-dark areas within the Hevelius formation.

4.6. Scenario 3: A Lossy Layer at Depth

[29] In this scenario a layer of pure highland ejecta, of thickness h and loss tangent tan δ, overlies mare basalt or a deep, mixed zone of highland and mare debris (Figure 9). Because the surface layer is dominated by highland material, the radar and multispectral properties (i.e., inferred TiO_2 abundance) can be uncorrelated. We obtain a maximum possible depth for the lossy layer by assuming that there is no significant surface echo ($K \sim 0$). The ratio of subsurface returns for the two-layer and one-layer cases is

$$\frac{\sigma^0_{\text{cryptomare}}}{\sigma^0_{\text{ejecta}}} = \frac{\frac{T\cos\theta}{4\alpha}\left[1-\exp\left(\frac{-4\alpha h}{\cos\theta}\right)\right]\sigma_1^0 + \frac{T\cos\theta}{4\alpha}\left[-\exp\left(\frac{-4\alpha h}{\cos\theta}\right)\right]\sigma_2^0}{\left(\frac{T\cos\theta}{4\alpha}\right)\sigma_1^0}, \tag{8}$$

where σ_1^0 and σ_2^0 are the integrated backscattering coefficients of the rock populations for layers 1 and 2. This expression simplifies to

$$\frac{\sigma^0_{\text{cryptomare}}}{\sigma^0_{\text{ejecta}}} = 1 - \left[\exp\left(\frac{-4\alpha h}{\cos\theta}\right)\right]\left(\frac{\sigma_2^0}{\sigma_1^0}+1\right). \tag{9}$$

The depth of burial has a maximum value when layer 2 has very low backscatter (high tan δ or low rock population). Substituting (3) into (9) and setting $\sigma_2^0 = 0$,

$$h_{\max} = \frac{-\ln\left(1-\frac{\sigma^0_{\text{cryptomare}}}{\sigma^0_{\text{ejecta}}}\right)}{4\pi\sqrt{\varepsilon'}\tan\delta}\lambda\cos\theta. \tag{10}$$

[30] For the Cruger-Sirsalis region the average shift in backscatter, relative to the inner Hevelius formation, is about 5 dB. Using a radar incidence angle of 60°, a real dielectric constant of 2.8, and a free space wavelength of 0.7 m, we obtain

$$h_{\max}(\text{meters}) = 0.0109/\tan\delta. \tag{11}$$

As noted in section 4.3, the lowest-measured loss tangent for lunar material is 0.0002, which yields $h_{\max}$ = 55 m; a value of tan δ = 0.001 yields $h_{\max}$ = 11 m. If the surface-scattering component increases ($K > 0$), the cutoff depth becomes smaller for any given loss tangent. As the mixed highland-mare layer reflects more of the incident signal ($\sigma_2^0 > 0$), the maximum possible depth of burial also decreases.

[31] We conclude that a lossy layer of mixed mare and highland material, at depths <55 m beneath low-loss highland material, is a reasonable explanation for the lower 70 cm and 7.5 m radar backscatter values in the Cruger-Sirsalis region and possibly in other radar-dark portions of the Hevelius formation. Since basin ejecta layers may be hundreds of meters thick [*McGetchin et al.*, 1973; *Howard et al.*, 1974], this cutoff depth represents the proximity to the visible surface of a mixed zone of much greater overall thickness (again, consistent with the 7.5 m echoes, which may penetrate to depths of hundreds of meters). A buried layer at depths of a few tens of meters is plausible but requires that the loss tangent of the Orientale-derived ejecta be closer to the low end of the measured range (0.0002). If the average value of tan δ is 0.001 or greater, then the mixed zone must come within <10 m of the surface over a large region.

5. Geologic Synthesis

[32] In this section we use the 70 cm radar maps and Clementine data to map the near-surface regolith properties across the Orientale-Procellarum region. One useful parameter for this work is the circular polarization ratio μ_c (SC power/OC power), which can highlight subtle shifts in the scattering properties of the regolith, especially the radar-dark haloes (Figure 10). Figure 11 shows a map of the major regolith units across the study region. We identify four terrain classes: (1) "ordinary" highland material comprising the Orientale ejecta blanket (black and white image base), (2) post-Orientale mare basalts (radar dark, low albedo, high FeO, and high TiO_2 relative to the terrae), exposed at the surface, including a small deposit in the floor of Rocca P crater (red), (3) radar-dark, low-μ_c, concentric haloes surrounding Imbrian, Eratosthenian, and Copernican impact craters and attributed to a rock-poor ejecta layer at least several meters thick [*Ghent et al.*, 2005] (green), and

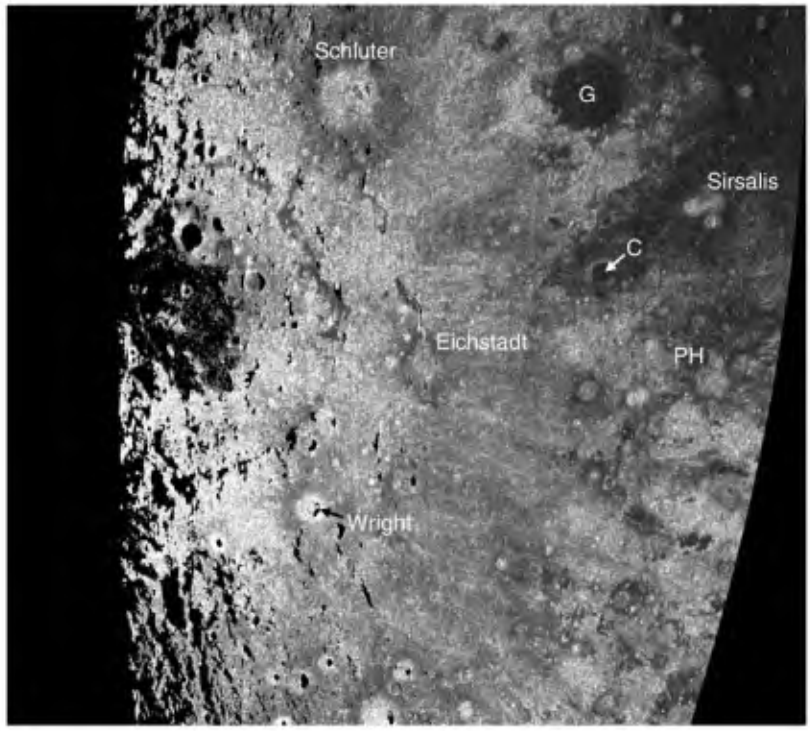

Figure 10. The 70 cm circular polarization ratio μ_c for the study region (0°–45°S, 55°–105°W). Image scale (black = 0.0; white = 1.0). Increasingly diffuse scattering from surface or subsurface rocks denoted by higher values. Diffuse scattering typically dominant at high incidence angles, so rough areas near the limb (left) have ratios near unity. G, Grimaldi; C, Cruger; PH, Prosper Henry.

(4) areas of low radar return and low μ_c, attributed to cryptomaria, along the western highland margin of Oceanus Procellarum, surrounding Cruger, southwest of Grimaldi and in patches toward the SE (yellow).

[33] One interesting feature of this map is the considerable extent of rock-poor ejecta from younger craters such as Schluter, Maunder, Eichstadt, Henry, Nicholson, Pettit, Focas, Sirsalis, the Copernican-age Sirsalis E, and two craters flanking Byrgius (Byrgius D to the west and Byrgius A to the east) [*Scott et al.*, 1977]. The haloes associated with Sirsalis and the superposed Sirsalis E affect a large area of our proposed cryptomaria but do not appear to extend across the entire region of low 70 cm return. The low-return halo of Prosper Henry crater is distinctly asymmetric, with a large lobe toward the north. The same pattern of asymmetry is reflected in the radar-bright, near-rim deposits, consistent with our assumption that the dark haloes are emplaced as distal crater ejecta [*Ghent et al.*, 2005]. The areas of moderately low μ_c, characterized by feathery margins, which extend radially from Montes cordillera, may reflect a decrease in near-surface rock abundance within the Hevelius formation.

[34] We thus propose that pre-Orientale mare basalts underlie the western highland margin of Oceanus Procellarum, the terrae northwest and southeast of Grimaldi basin, the southern floor of Riccioli crater, and the topographic low surrounding Cruger crater. There are also cryptomare patches to the southeast but not apparently to the south of Orientale. The total area of these cryptomare deposits within our study region is about 178×10^3 km^2, representing ~0.5% of the total lunar surface and a 2.7% increase in the previously mapped mare coverage (6.4×10^6 km^2 [*Horz et al.*, 1991]).

[35] All of the cryptomare units, however, lie outside of an arc approximately 700 km from the Orientale basin center. Combined with the multispectral observations cited in this study and in earlier work by *Mustard and Head* [1996], this suggests that the mixed mare-highland zone is covered by a highland-dominated layer that thins away from the basin center. This is reasonable, on the basis of models and measurements of impact ejecta deposition [e.g., *Moore et al.*, 1974]. The increasing thickness of the ejecta toward the basin center thus limits our ability to detect buried mare deposits. The true western extent of the ancient mare basalts remains uncertain, and our areal estimate represents a lower bound on the increase in total mare coverage of the Moon.

6. Conclusions

[36] We used new 70 cm wavelength radar images, collected using Arecibo Observatory and the Green Bank Telescope, and Clementine data to study cryptomare deposits east of Orientale basin. Earlier multispectral analyses showed that mare material is mixed with the highland terrain along the western margin of Oceanus Procellarum, leading to a detectable increase in the FeO and TiO_2 abundance of the regolith surface. The highland margin of western Procellarum is also characterized by low 70 cm radar returns, consistent with an increased regolith loss tangent due to ilmenite in the mare-derived material. The low 70 cm radar echo, however, persists well to the west of

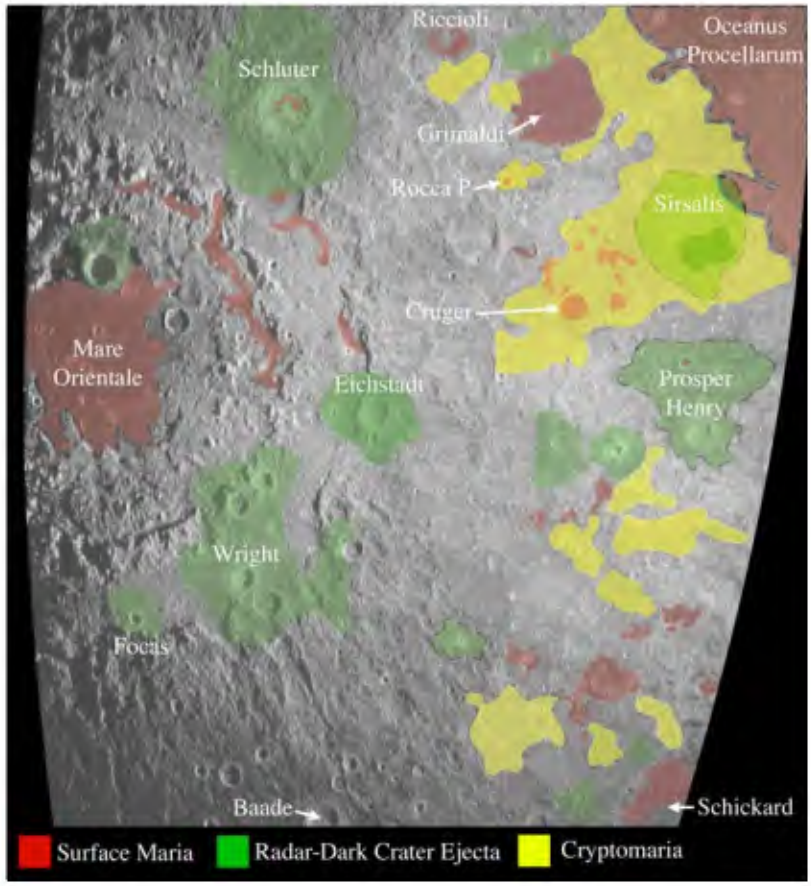

Figure 11. Sketch map of major near-surface physical-geochemical regolith units. Background black and white image base (identical to Figure 2) dominated by Orientale-derived, highland-rich ejecta. Mare basalts at the surface shown as red; rock-poor ejecta haloes of craters shown as green; cryptomaria shown as yellow. Estimate of the Sirsalis radar-dark halo reflected by large light green region surrounding Sirsalis. Radar-dark halo of Sirsalis E shown as dark green inset area. Uncertain contacts shown as dashed boundaries.

the mixed zone evident in multispectral data, and includes the region surrounding Cruger crater. It is likely that mare basalt, or a mixed zone of mare and highland material, exists at depth across the region and only reaches the visible surface near the western Procellarum margin. The plausible depth to this mixed zone is dependent upon the loss tangent of the overlying pure highland ejecta. If Orientale ejecta is dominated by low-loss anorthosite, then the mixed zone could lie at depths of up to several tens of meters. We propose that pre-Orientale mare deposits flooded the region between Cruger and Oceanus Procellarum and also patches west and northwest of Humorum basin. These deposits comprise a minimum 2.7% increase in the areal coverage of known lunar mare basalts.

[37] **Acknowledgments.** Helpful reviews were provided by R. Greeley and B. Cooper. The authors thank the staff at Cornell University, Arecibo Observatory, and the Green Bank Telescope for invaluable assistance in collecting the new lunar radar data. In particular, we thank D. Campbell, J. Margot, M. Nolan, and F. Ghigo. J. Chandler (SAO) provided the ephemeris files for the observations. The Arecibo Observatory is part of the National Astronomy and Ionosphere Center, which is operated by Cornell University under a cooperative agreement with the National Science Foundation (NSF) and with support from NASA. The Green Bank Telescope is part of the National Radio Astronomy Observatory, a facility of the NSF operated under cooperative agreement by Associated Universities, Inc. This work was supported in part by a grant from the NASA Planetary Geology and Geophysics Program.

References

Antonenko, I., J. W. Head, J. F. Mustard, and B. R. Hawke (1995), Criteria for the detection of lunar cryptomaria, *Earth Moon Planets*, *69*, 141–172.

Blewett, D. T., B. R. Hawke, P. G. Lucey, G. J. Taylor, R. Jaumann, and P. D. Spudis (1995), Remote sensing and geologic studies of the Schiller-Schickard region of the Moon, *J. Geophys. Res.*, *100*, 16,959–16,977.

Bussey, D. B. J., and P. D. Spudis (2000), Compositional studies of the Orientale, Humorum, Nectaris, and Crisium lunar basins, *J. Geophys. Res.*, *105*, 4235–4244.

Campbell, B. A. (2002), *Radar Remote Sensing of Planetary Surfaces*, Cambridge Univ. Press, New York.

Campbell, B. A., R. E. Arvidson, and M. K. Shepard (1993), Radar polarization properties of volcanic and playa surfaces: Applications to terrestrial remote sensing and Magellan data interpretation, *J. Geophys. Res.*, *98*, 17,099–17,114.

Campbell, B. A., B. R. Hawke, and T. W. Thompson (1997), Long-wavelength radar studies of the lunar maria, *J. Geophys. Res.*, *102*, 19,307–19,320.

Carrier, W. D., G. R. Olhoeft, and W. Mendell (1991), Physical properties of the lunar surface, in *Lunar Sourcebook*, pp. 475–567, Cambridge Univ. Press, New York.

Ghent, R. R., D. Leverington, B. A. Campbell, B. R. Hawke, and D. Campbell (2005), Earth-based observations of radar-dark crater haloes on the Moon: Implications for regolith properties, *J. Geophys. Res.*, *110*, E02005, doi:10.1029/2004JE002366.

Gillis, J. J., B. L. Joliff, and R. C. Elphic (2003), A revised algorithm for calculating TiO_2 from Clementine UVVIS data: A synthesis of rock, soil, and remotely sensed TiO_2 concentrations, *J. Geophys. Res.*, *108*(E2), 5009, doi:10.1029/2001JE001515.

Hagfors, T. (1967), A study of the depolarization of lunar radar echoes, *Radio Sci.*, *2*, 445–465.

Hagfors, T. (1970), Remote probing of the Moon by infrared and microwave emissions and radar, *Radio Sci.*, *5*, 189–227.

Hawke, B. R., C. A. Peterson, P. G. Lucey, G. J. Taylor, D. T. Blewett, B. A. Campbell, and P. D. Spudis (1993), Remote sensing studies of the terrain northwest of Humorum basin, *Geophys. Res. Lett.*, *20*, 419–422.

Hawke, B. R., J. J. Gillis, T. A. Giguere, D. T. Blewett, D. J. Lawrence, P. G. Lucey, G. A. Smith, P. D. Spudis, and G. J. Taylor (2004), Remote sensing and geologic studies of the Balmer region of the Moon, *Lunar Planet. Sci.*, *XXXV*, Abstract 1190.

Horz, F., R. Grieve, G. Heiken, P. Spudis, and A. Binder (1991), Lunar surface processes, in *Lunar Sourcebook*, pp. 61–111, Cambridge Univ. Press, New York.

Howard, K. A., D. E. Wilhelms, and D. H. Scott (1974), Lunar basin formation and highland stratigraphy, *Rev. Geophys.*, *12*, 309–327.

Lucey, P. G., B. C. Bruno, and B. R. Hawke (1991), Preliminary results of imaging spectroscopy of the Humorum basin region of the Moon, *Proc. Lunar Planet Sci. Conf.*, *21st*, 391–404.

Lucey, P. G., D. T. Blewett, and B. L. Joliff (2000), Lunar iron and titanium abundance algorithms based on final processing of Clementine ultraviolet-visible images, *J. Geophys. Res.*, *105*, 20,297–20,306.

McGetchin, T. R., M. Settle, and J. W. Head (1973), Radial thickness variations in impact crater ejecta: Implications for lunar basin deposits, *Earth Planet. Sci. Lett.*, *20*, 226–236.

Moore, H. J., C. A. Hodges, and D. H. Scott (1974), Multiringed basins—Illustrated by Orientale and associated features, *Proc. Lunar Planet. Sci. Conf.*, *5th*, 71–100.

Mustard, J. F., and J. W. Head (1996), Buried stratigraphic relationships along the southwestern shores of Oceanus Procellarum: Implications for early lunar volcanism, *J. Geophys. Res.*, *101*, 18,913–18,925.

Olhoeft, G. R., and D. W. Strangway (1975), Dielectric properties of the first 100 meters of the Moon, *Earth Planet. Sci. Lett.*, *24*, 394–404.

Schaber, G. G., T. W. Thompson, and S. H. Zisk (1975), Lava flows in Mare Imbrium: An evaluation of anomalously low Earth-based radar reflectivity, *Moon*, *13*, 395–423.

Schultz, P. H., and P. D. Spudis (1979), Evidence for ancient mare volcanism, *Proc. Lunar Planet. Sci. Conf.*, *10th*, 2899–2918.

Scott, D. H., J. F. McCauley, and M. N. West (1977), Geologic map of the west side of the Moon, *U.S. Geol. Surv. Misc. Geol. Invest. Map, I-1034*.

Shoemaker, E. M., and E. C. Morris (1968), Size-frequency distribution of fragmental debris, in *Surveyor Project Final Report*, *NASA Tech. Rep.*, *32-1265*, 86–102.

Shorthill, R. W. (1973), Infrared atlas charts of the eclipsed Moon, *Moon*, *7*, 22–45.

Stacy, N. J. S. (1993), High-resolution synthetic aperture radar observations of the Moon, Ph.D. thesis, Cornell Univ., Ithaca, N. Y.

Thompson, T. W. (1978), High resolution lunar radar map at 7.5 m wavelength, *Icarus*, *36*, 174–188.

Ulaby, F. T., R. K. Moore, and A. K. Fung (1982), *Microwave Remote Sensing*, Addison-Wesley, Boston, Mass.

Wilhelms, D. E. (1987), The geologic history of the Moon, *U.S. Geol. Surv. Prof.*, *1348*.

Zisk, S. H., G. H. Pettengill, and G. W. Catuna (1974), High-resolution radar maps of the lunar surface at 3.8 cm wavelength, *Moon*, *10*, 17–50.

B. A. Campbell, Center for Earth and Planetary Studies, Smithsonian Institution, MRC 315, P.O. Box 37012, Washington, DC 20013-7012, USA. (campbellb@si.edu)

B. R. Hawke, Hawai'i Institute of Geophysics and Planetology, University of Hawai'i at Manoa, 1680 East-West Road, Honolulu, HI 96822, USA.